



HAL
open science

Polarization-oriented LiNbO₃ nanocrystals by femtosecond laser irradiation in LiO₂–Nb₂O₅–SiO₂–B₂O₃ glasses

Elisa Muzi, Maxime Cavillon, Matthieu Lancry, François Brisset, Benjamin Sapaly, Davide Janner, Bertrand Pournellec

► To cite this version:

Elisa Muzi, Maxime Cavillon, Matthieu Lancry, François Brisset, Benjamin Sapaly, et al.. Polarization-oriented LiNbO₃ nanocrystals by femtosecond laser irradiation in LiO₂–Nb₂O₅–SiO₂–B₂O₃ glasses. *Optical Materials Express*, 2021, 11 (4), pp.1313-1320. 10.1364/ome.417461. hal-03418512

HAL Id: hal-03418512

<https://hal.science/hal-03418512v1>

Submitted on 7 Nov 2021

HAL is a multi-disciplinary open access archive for the deposit and dissemination of scientific research documents, whether they are published or not. The documents may come from teaching and research institutions in France or abroad, or from public or private research centers.

L'archive ouverte pluridisciplinaire **HAL**, est destinée au dépôt et à la diffusion de documents scientifiques de niveau recherche, publiés ou non, émanant des établissements d'enseignement et de recherche français ou étrangers, des laboratoires publics ou privés.

Important Notice to Authors

Attached is a PDF proof of your forthcoming article in Optical Materials Express. The article Manuscript ID is 417461. *No further processing of your paper will occur until we receive your response to this proof.*

Note: *Excessive proof corrections submitted by the author can result in significant delays to publication. Please include only essential changes that might be needed to address any shortcomings noticed in the proof-preparation process.*

Author Queries

Please answer these queries by marking the required corrections at the appropriate point in the text or referring to the relevant line number in your PDF proof.

Q1	The funding information for this article has been generated using the information you provided to OSA at the time of article submission. Please check it carefully. If any information needs to be corrected or added, please provide the full name of the funding organization/institution as provided in the Crossref Open Funder Registry (https://search.crossref.org/funding).
----	---

Other Items to Check

- Please note that the original manuscript has been converted to XML prior to the creation of the PDF proof, as described above. The PDF proof was generated using LaTeX for typesetting. The placement of your figures and tables may not be identical to your original paper.
- Please carefully check all key elements of the paper, particularly the equations and tabular data.
- Author list: Please make sure all authors are presented, in the appropriate order, and that all names are spelled correctly.
- If you need to supply new or replacement figures, please upload each figure as an individual PDF file at the desired final figure size. The figure must fit inside the margins of the manuscript, i.e., width no more than 5.3 inches (or 13.46 cm). Confirm the quality of the figures and upload the revised files when submitting proof corrections.

Polarization-oriented LiNbO₃ nanocrystals by femtosecond laser irradiation in LiO₂–Nb₂O₅–SiO₂–B₂O₃ glasses

ELISA MUZI,^{1,2,*} MAXIME CAVILLON,¹  MATTHIEU LANCRY,¹ 
FRANÇOIS BRISSET,¹ BENJAMIN SAPALY,¹ DAVIDE JANNER,² AND
BERTRAND POUHELLEC¹ 

¹*Institut de Chimie Moléculaire et des Matériaux d'Orsay (ICMMO), Université Paris-Saclay, CNRS, 91405 Orsay, France*

²*Department of Applied Science and Technology (DISAT), Politecnico di Torino, 10129 Torino, Italy*

**elisa.muzy@universite-paris-saclay.fr*

Abstract: This work investigates the role of a B₂O₃ addition (up to 21 mole %) into a lithium niobium silicate glass matrix, focusing on the orientational dependency of second harmonic generation (SHG), induced after femtosecond laser irradiation. We detected the sharp emission of light at 515 nm, characteristic of SHG, in both static and scanning configurations, using pulse energy, repetition rate, and laser polarization as varying parameters. Among the results to highlight, the SHG signature appears within a few seconds in highly doped B₂O₃ glass, i.e., one order of magnitude smaller than in B₂O₃-free glass. Additionally, we found that the orientability of the polar axis of LiNbO₃ nanocrystals by writing laser polarization can be obtained in glasses when SiO₂ is substituted with B₂O₃. These preliminary results open the door to the fabrication of crystal / glass based photonic devices with lower laser power deposited and much faster crystallization kinetics.

© 2021 Optical Society of America under the terms of the [OSA Open Access Publishing Agreement](#)

1. Introduction

Femtosecond (fs) laser direct writing (FLDW) is a powerful and versatile tool enabling a large variety of optical components to be fabricated in transparent materials such as glasses (e.g. Bragg gratings, waveguides, graded index lenses, birefringent optics) [1–3]. In addition to surface modifications, the femtosecond laser irradiation has allowed the 3D-nanostructuring of optical properties induced by permanent effects on material structure. By controlling the fs-laser parameters (e.g. pulse energy, repetition rate, scanning speed, polarization), it becomes possible to induce crystallization inside a glass substrate with a high spatial selectivity (few tens of μm³ or less). Some examples of crystals induced by FLDW in glasses can be found in the recent review of Komatsu et al. [4], among which we can cite β-BaB₂O₄ [5], Ba₂TiSi₂O₈ [6], or LiNbO₃ [7].

A particular focus is about fs-laser crystallization of LiNbO₃ in silicate matrix, a crystal that allows many applications in different fields because of its properties: ferroelectricity, pyroelectricity, piezoelectricity and a large second order susceptibility. In particular, because of its axial symmetry, the second order susceptibility tensor ($\chi^{(2)}$) of LiNbO₃ crystal is such that its nonlinear coefficient value along the polar axis ($d_{33} = 34.4$ pm/V [8,9]) is much greater than the nonlinear coefficients values along the other axes ($d_{31} = 4.88$ pm/V, $d_{22} = 2.58$ pm/V [8,9]). Therefore, it presents an angular dependence of $\chi^{(2)}$ -related processes, such as second harmonic generation (SHG). This translates into a modulation of the SHG signal during FLDW that occurs when the crystals can be oriented along the direction of laser polarization.

To produce crystallization by FLDW, the typical glass matrix used in previous works is composed of 33%Li₂O – 33%Nb₂O₅ – 34%SiO₂ (LNS) (molar %) [7,10]. Although interesting results have been published, the impact of the glass matrix has not been studied extensively yet.

In particular, if SiO_2 is partially substituted with B_2O_3 , the impact on the crystallization rate can drastically increase, unlocking in such a way the industrial potential of this direct writing technique. Indeed, the incorporation of B_2O_3 into the glass matrix is of interest as it is expected to lower the glass transition temperature and, thus, to improve the kinetics of LiNbO_3 crystallization compared for LNS glass [11–14].

In this work, we report on the impact of LiNbO_3 crystallization by FLDW by adding a significant amount of B_2O_3 in the glass matrix (through modification of the starting glass batch composition). We revealed the creation of polarization dependent $\chi^{(2)}$ by the SHG detection and confirmed this is related to LiNbO_3 nanocrystals by electron backscattered diffraction (EBSD) measurements. As a reference, we start with the crystallization of a typical LNS glass. We, then, intend to analyze the impact on fs-laser irradiation on glass crystallization, when SiO_2 is partly substituted with B_2O_3 . More specifically, we aim at determining whether it is possible to induce tunable SHG angular modulation in these glassy matrices and to identify the orientation of the laser-induced nanocrystals in these borosilicate glass matrices compared to LNS glass (i.e., B_2O_3 -free glass).

2. Method

Four glasses, with increasing B_2O_3 content up to 21%, were fabricated using melt-quenching technique. Compositions and labels are reported in the Table 1. A powder mixture of 30 grams per batch composed of SiO_2 (99.9%, SERLABO), H_3BO_3 (99.5%, PROLABO), Li_2CO_3 (99.9%, SIGMA ACS reagent) and Nb_2O_5 (99.5%, STREM CHEMICALS) powders in stoichiometric amount, was first homogenized using acetone. The mixed powder was then placed inside a platinum crucible and dried at 200°C for 2 hours before increasing the temperature at a heating rate of $5^\circ\text{C}/\text{min}$ up to 1000°C . The mixed powder remained at this temperature for 1 hour. After that, to obtain the melting, the temperature was increased to 1400°C for LNS34 and 1350°C for LNS27B7, LNS20B14, LNS13B21 at a heating rate of $10^\circ\text{C}/\text{min}$. Finally, the molten mixture was quenched between two metal plates preheated at around 350°C and maintained at this temperature for about 30 minutes.

Table 1. Glass labels and batch compositions

Glass label	Glass batch composition (mol%)
LNS34	33% LiO_2 – 33% Nb_2O_5 – 34% SiO_2
LNS27B7	33% LiO_2 – 33% Nb_2O_5 – 27% SiO_2 – 7% B_2O_3
LNS20B14	33% LiO_2 – 33% Nb_2O_5 – 20% SiO_2 – 14% B_2O_3
LNS13B21	33% LiO_2 – 33% Nb_2O_5 – 13% SiO_2 – 21% B_2O_3

The obtained glasses had the shape of a slab of about 1 mm thickness. For laser irradiation, samples were double side polished to reach optical quality and then they were placed on the FLDW system that comprises a motorized translation stage and a commercial femtosecond laser (Satsuma, Amplitude Systèmes Ltd, $\lambda = 1030$ nm, pulse duration = 250 fs). Each irradiation was performed by focusing the laser beam approximately $240\ \mu\text{m}$ below the sample top surface using a 0.6 numerical aperture (NA) aspheric lens. We choose this focusing depth to avoid any surface ablation when scanning over long distances and to avoid heterogenous nucleation preferentially triggered at the surface.

The translation stage enables a displacement in the XY plane, while the laser beam propagation direction is along the Z direction as depicted in Fig. 1(a). Three different laser polarization configurations referenced relative to the laser writing direction, along the Y-axis, were used: parallel: parallel (Y_y), at 45° (Y_{45}) and perpendicular (Y_x) to it. The SHG intensity was recorded in transmission using a spectrometer (Jaz, Ocean Optics) equipped with a multimode optical fiber

and a coupling lens to maximize light collection from the sample. A more detailed description of the setup is reported in Ref. [7].

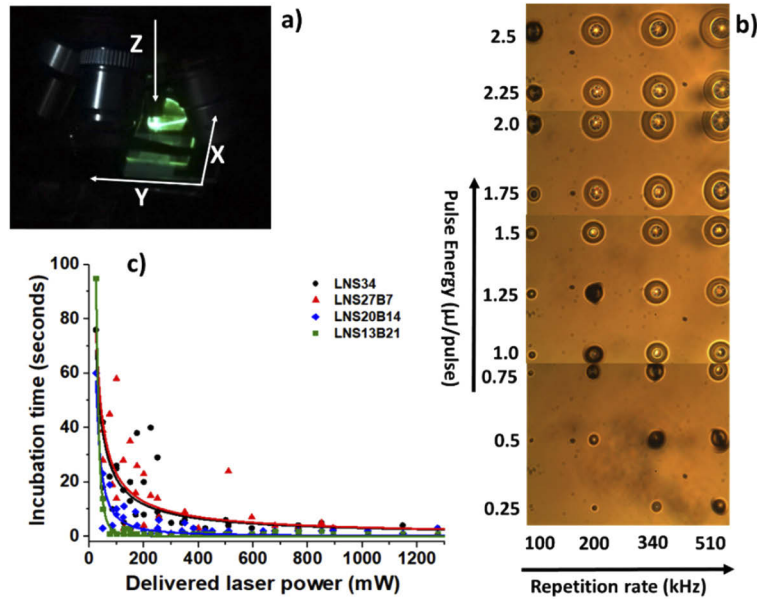


Fig. 1. a) Typical image of SHG detected after few seconds under static irradiation that corresponds to the end of the incubation time; b) Optical microscope image in transmission and white light of static irradiation until the onset of SHG of LNS34 glass sample with varying laser parameters; c) Incubation time as a function of the power (in mW) delivered by the laser in static conditions for four glass compositions. Laser conditions used: $\lambda = 1030$ nm, $NA = 0.6$, $f = 200$ kHz, focus depth = $240 \mu\text{m}$ in air. In Fig. 1(c), each data set was fitted with a power law (ax^b); the latter only serves as a guide-to-the-eye.

We started by performing a static irradiation to investigate the influence of laser parameters during laser-induced crystallization. This experiment, carried out on each sample, served to determine the incubation time as a function of glass composition. The incubation time is the time taken, upon fs-laser irradiation, until the observation of the SHG signal ($\lambda_{\text{SHG}} = \lambda/2 = 515$ nm) and is indicative of the early birth of non-centrosymmetric crystals, typically LiNbO_3 is expected in our case [7]. At this stage, only two laser parameters were varied, i.e., the pulse energy, ranging from 0.25 to $2.5 \mu\text{J}$, in steps of $0.25 \mu\text{J}$ and the laser repetition rate, with values of 100 kHz, 200 kHz, 340 kHz, and 510 kHz. The laser polarization was fixed along the X-axis that is defined by the plane of laser compressor. The minimum incubation time to induce crystallization, found from the above experiments, is also needed for writing lines structures. First the laser was set in static mode for the minimum incubation time until green light was detected; then the laser scanning was started. Line writing parameters were set at a fixed repetition rate of 200 kHz and writing speed of $1 \mu\text{m/s}$ using different pulse energies ($0.25 \mu\text{J}$ to $2.0 \mu\text{J}$, step of $0.25 \mu\text{J}$). This was repeated for the three different laser polarization configurations to assess their influence on the crystal orientation, namely parallel (Y_y), at 45° (Y_{45}) and perpendicular (Y_x).

For each written line, we measured the SHG intensity in the XY plane according to the azimuthal angle (θ) of the probe beam polarization, up to 180° starting from the polarizer reference position in correspondence of 0° , i.e., along X. The probe beam propagation direction was set perpendicular to the XY plane and its electric field direction was parallel to this plane.

In our samples, the SHG intensity was measured in transmission mode with the fundamental beam (1030 nm) propagating perpendicularly to the sample XY plane at pulse energy = $0.1 \mu\text{J/pulse}$.

154 The spot size (diameter) of the probing beam was approximately 30 μm , well overlapping each
155 laser track during SHG measurements. The repetition rate during the measurement was set at
156 100 kHz. The transmitted SHG light (515 nm) was recorded after passing an IR low pass filter
157 mounted before the spectrometer collector.

158 Finally, to investigate the correlation between the laser induced microstructure and the SHG
159 response, we proceeded with an analysis at field-emission scanning electron microscope (FEG-
160 SEM ZEISS SUPRA 55 VP) with electron backscattered diffraction (EBSD) detector (TSL-EDAX
161 Velocity Camera and OIM Analysis software).

162 3. Results and discussion

163
164 In Fig. 1, we report respectively: a) the SHG signal detected upon irradiation, b) the laser induced
165 modifications observation under optical microscope with varying conditions, and c) incubation
166 times measured for each glass sample under static irradiation. In particular, Fig. 1(b) illustrates
167 the dependence of the laser affected zone on both pulse energy (E_p) and repetition rate (RR). As
168 the deposited power ($P = RR \times E_p$) increases, the area of the modified region becomes wider than
169 the spot size, which is characteristic of thermal accumulation in and around the focal spot (of
170 radius $w_0 \sim 1.2\lambda/(2NA) \sim 1 \mu\text{m}$). Figure 1(c) shows that the measured incubation time decreases
171 as the delivered power P increases. For similar experimental conditions, these measurements
172 clearly indicate the tendency for LNS13B21 glass to crystallize at a much higher rate compared
173 to other glasses. For example, at a delivered power of 100 mW, LNS13B21 sample exhibits an
174 incubation time of ~ 1 second, while it is of ~ 10 seconds for LNS20B14 and ~ 20 seconds for
175 both LNS27B7 and LNS34, as represented in Fig. 1(c). In term of laser-affected volume, we
176 observe that both laser track width and length (measured within the cross section) increase along
177 with the pulse energy. This behavior is characteristic of more heat deposited inside the glass
178 upon irradiation and it is in agreement with results from Fig. 11 in Ref. [7].

179 To assess the effect of the orientation of the writing laser polarization on the crystals, we
180 investigated the angular dependency of the SHG intensity. All the measured values, as a function
181 of the azimuthal orientation of the probing linear polarization, were normalized relative to their
182 highest value as shown in Fig. 2. Here we compared two writing configuration schemes: Y_x and
183 Y_{45} . In particular, we choose to represent those relative to two characteristics pulse energies, i.e.,
184 0.5 μJ and 1.25 μJ , because of important SHG trends variations that are visible in Fig. 2(a) and
185 2(b), for the four investigated glasses. For the lowest energy value, a strong SHG modulation is
186 found with an azimuth- θ of 90° for all glasses. For pulse energy of 1.25 μJ , the evidence of SHG
187 “directionality” is strongly reduced for all four samples, as it is more easily visible from the polar
188 representations referring to LNS1B21 sample, reported in Fig. 2(c). Here we note the occurrence
189 of a second maximum on the SHG (θ) curve along the polarization direction.

190 More specifically, from Fig. 2, we observe that at the lowest energy (0.5 $\mu\text{J}/\text{pulse}$), the
191 normalized SHG intensity (I/I_{max}) follows a sinusoidal behavior with a strong contrast ($(I_{\text{max}} -$
192 $I_{\text{min}})/(I_{\text{max}} + I_{\text{min}})$) up to 0.9 for LNS20B14. We note a maximum for a direction perpendicular to
193 the laser polarization i.e., 90° and 135° for Y_x and Y_{45} configurations, respectively. In contrast
194 the minimum SHG is found for a probing angle perpendicular to the maximum one. This is in
195 agreement with Ref. [10], where the polar axis of LiNbO_3 is oriented perpendicularly to the
196 laser polarization. Interestingly, this behavior is preserved even after a large substitution of SiO_2
197 with B_2O_3 .

198 As the pulse energy is increased, from 0.5 to 1.25 μJ , the SHG intensity profile becomes more
199 “isotropic”, which could be caused by the presence of several crystalline textures with different
200 orientations [15]. Indeed, from Fig. 2(c) we can see that the low energy texture (population
201 leading to SHG_{max} for θ perpendicular to writing polarization) is still appearing at 1.25 μJ .
202 However, there is another contribution that appears in the SHG (θ) response, and is indicative of
203 a second texture (i.e., a second population of LiNbO_3 crystals with a preferential orientation).
204

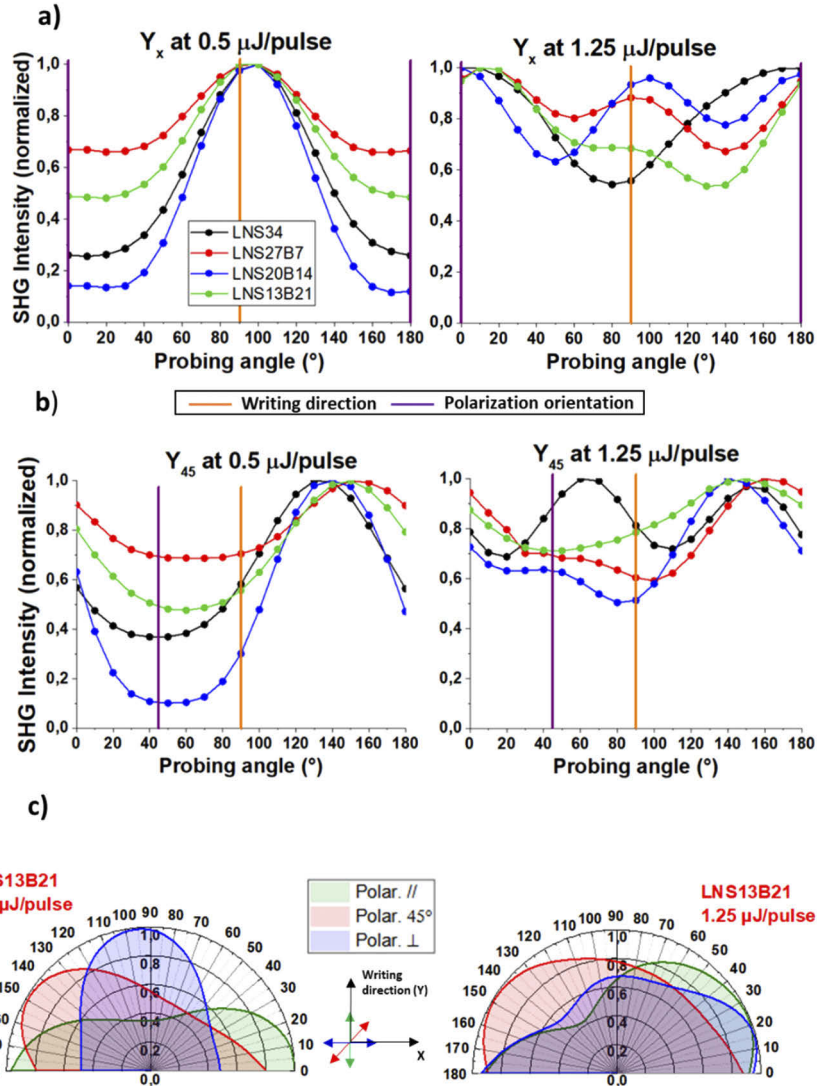


Fig. 2. Normalized SHG intensity for four glass compositions as a function of probing polarization angle in the XY plane as defined in the text, a) for the four glass samples, configuration Y_x at two pulse energies: $0.5 \mu\text{J/pulse}$ and $1.25 \mu\text{J/pulse}$; b) same as a) but for the Y_{45} configuration. Both the writing direction and the laser polarization during writing are reported on each graph; c) polar representations for LNS13B21 glass for $0.5 \mu\text{J/pulse}$ and $1.25 \mu\text{J/pulse}$ with three configurations: Y_y , Y_{45} and Y_x (the polarization orientations with respect to writing direction are indicated by double headed arrows in the coordinates of the reference system).

256 This is also clear with the configuration Y_{45} for which there is no maximum in the direction of
 257 writing.

258 One could expect the minima and maxima of the SHG modulation to be positioned exactly 90°
 259 apart from the laser polarization. However, a slight departure from this angle is observed, and
 260

261
262
263
264
265
266
267
268
269
270
271
272
273
274
275
276
277
278
279
280
281
282
283
284
285
286
287
288
289
290
291
292
293
294
295
296
297
298
299
300
301
302
303
304
305
306

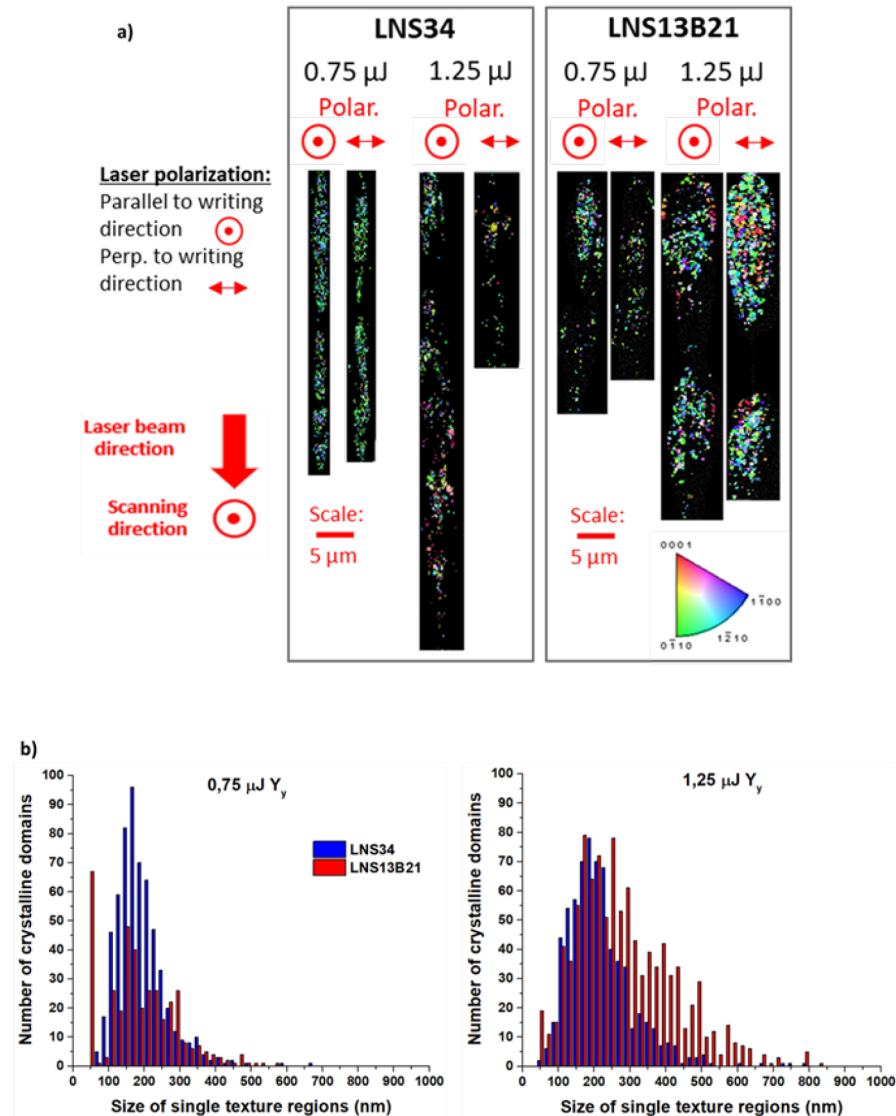


Fig. 3. a) Electron Back Scatter Diffraction (EBSD) micrographs of the laser track cross sections for both LNS34 and LNS13B21 glass samples, for two pulse energies (0.75 μJ /pulse and 1.25 μJ /pulse) and with laser polarization either parallel or perpendicular to the scanning direction. The inverse pole figure (IPF) color code is based on LiNbO_3 space group, with coding along the laser polarization direction; b) Size distribution of single texture regions for LNS34 and LNS13B21 for the Y_y configuration and two different pulse energies (0.75 μJ and 1.25 μJ). Irradiation conditions: $\lambda = 1030$ nm, NA = 0.6, f = 200 kHz, focus depth = 240 μm in air, writing speed = 1 $\mu\text{m/s}$.

307 may be due to an asymmetric orientational writing effect as previously observed at low speeds
308 (1 $\mu\text{m/s}$, similar to this work) in LNS glass [15].

309 Finally, to validate the presence of the LiNbO_3 crystals and to study their orientation inside
310 the laser track cross sections, electron backscattered diffraction (EBSD) analysis was performed
311 on LNS34 and LNS13B21 samples [16,17]. The results are presented in Fig. 3(a).

312 We first observed that LiNbO_3 nanocrystals were effectively precipitated. Secondly, from the
313 inverse pole figure (IPF) color code, the crystal c axis (along the 0001 direction) is found to be
314 oriented perpendicular to the laser polarization (absence of red color on the EBSD map).

315 This is obviously the case at the lowest pulse energy, whereas at higher energies crystal c axis
316 orientation is observed to vary and be only partially oriented along the polarization direction.
317 Note that these observations are in agreement with the SHG experiments: at low pulse energies
318 the crystals are well oriented with their c axis perpendicular to the writing laser polarization
319 and corresponding to a maximum SHG contrast with a nearly single texturation. However, at
320 higher pulse energies, a part of the nanocrystals population exhibit c axis orientation along the
321 polarization leading to a more spatially distributed (hence isotropic) SHG response.

322 From the EBSD data (Fig. 3(a)) we could distribution of single texture regions of nanocrystals
323 (assuming they are spherical) within the investigated laser track area. In Fig. 3(b), we report this
324 distribution for LNS34 and LNS13B21 for the Y_y configuration and two different pulse energies
325 (0.75 μJ and 1.25 μJ). At the highest pulse energy (1.25 μJ in this comparison) we observe the
326 tendency to form larger regions with same textures compared to the low energy conditions (0.75
327 μJ , 20 nm – 300 nm diameter range).

328 4. Conclusion

329 In this work, we demonstrated that tunability of SHG in lithium niobate silicate glass can be
330 extended to the borosilicate glass family, through an adequate control of the laser parameters.
331 More specifically, the substitution of SiO_2 with B_2O_3 is found to be advantageous as it promotes
332 faster crystallization of LiNbO_3 crystals while preserving the tunability of SHG. The latter is
333 related to the larger SHG response along the c axis of the crystals, which is preferentially aligned
334 perpendicular to the laser polarization at low pulse energy. Currently, the LiNbO_3 orientation
335 is understood as being due to alignment of the larger linear susceptibility matrix element (\perp
336 to c axis) with the electric field [18]. We also observe that LNS13B21 glass exhibits a shorter
337 incubation time and thus likely a faster crystal growth with respect to LNS34 that may explain the
338 larger crystals at 1.25 μJ , and more experiments are ongoing to confirm this hypothesis. Several
339 key properties of the written structures related to photonic devices fabrication will be investigated
340 in the future, including refractive index changes and birefringence response.

341 **Funding.** Compagnia di San Paolo (Joint Research Program); Agence Nationale de la Recherche (CHARMMAT
342 ANR-11-LABX-0039). Q1

343 **Acknowledgments.** This work was supported by the French National Research Agency under the program
344 CHARMMAT ANR-11-LABX-0039-grant. Elisa Muzi and Davide Janner also acknowledge financial support from
345 Compagnia di S. Paolo through the Joint Research Program.

346 **Disclosures.** The authors declare no conflicts of interest.

347 References

- 348
- 349 1. R. R. Gattass and E. Mazur, "Femtosecond laser micromachining in transparent materials," *Nat. Photonics* **2**(4),
350 219–225 (2008).
 - 351 2. J. Habel, T. Boilard, J. S. Freniere, F. Trepanier, and M. Bernier, "Femtosecond FBG written through the coating for
352 sensing applications," *Sensors* **17**(11), 2519 (2017).
 - 353 3. T. T. Fernandez, M. Sakakura, S. M. Eaton, B. Sotillo, J. Siegel, J. Solis, Y. Shimotsuma, and K. Miura, "Bespoke
354 photonic devices using ultrafast laser driven ion migration in glasses," *Prog. Mater. Sci.* **94**, 68–113 (2018).
 - 355 4. T. Komatsu and T. Honma, "Laser patterning and growth mechanism of orientation designed crystals in oxide glasses:
356 A review," *J. Solid State Chem.* **275**, 210–222 (2019).
- 357

- 358
359
360
361
362
363
364
365
366
367
368
369
370
371
372
373
374
375
376
377
378
379
380
381
382
383
384
385
386
387
388
389
390
391
392
393
394
395
396
397
398
399
400
401
402
403
404
405
406
407
408
5. K. Miura, J. Qiu, T. Mitsuyu, and K. Hirao, "Space-selective growth of frequency-conversion crystals in glasses with ultrashort infrared laser pulses," *Opt. Lett.* **25**(6), 408–410 (2000).
 6. B. Zhu, Y. Dai, H. Ma, S. Zhang, G. Lin, and J. Qiu, "Femtosecond laser induced space-selective precipitation of nonlinear optical crystals in rare-earth-doped glasses," *Opt. Express* **15**(10), 6069–6074 (2007).
 7. J. Cao, M. Lancry, F. Brisset, L. Mazerolles, R. Saint-Martin, and B. Pommellec, "Femtosecond laser-induced crystallization in glasses: growth dynamics for orientable nanostructure and nanocrystallization," *Cryst. Growth Des.* **19**(4), 2189–2205 (2019).
 8. M. J. Weber, ed., *CRC Handbook of Laser Science and Technology* (CRC Press, 1986), Vol. Optical materials, Part 1: Nonlinear Optical Properties/Radiation damage.
 9. R. S. Klein, G. E. Kugel, A. Maillard, and K. Polgar, "Considerations of angular acceptance and non-linear optical coefficient measurements by second harmonic generation in LiNbO₃ crystals," *Ferroelectrics* **296**(1), 57–66 (2003).
 10. J. Cao, L. Mazerolles, M. Lancry, F. Brisset, and B. Pommellec, "Modifications in lithium niobium silicate glass by femtosecond laser direct writing: morphology, crystallization, and nanostructure," *J. Opt. Soc. Am. B* **34**(1), 160–168 (2017).
 11. M. P. Fernandes Graca and M. Almeida, "Glass ceramics with para, anti or ferroelectric active phases", in *Advances in Ceramics - Electric and Magnetic Ceramics, Bioceramics, Ceramics and Environment* (IntechOpen, 2011).
 12. A. Faeghi-Nia, V. K. Marghussian, and E. Taheri-Nassaj, "Effect of B₂O₃ on crystallization behavior and microstructure of MgO–SiO₂–Al₂O₃–K₂O–F glass–ceramics," *Ceram. Int.* **33**(5), 773–778 (2007).
 13. G. Ferlat, A. P. Seitsonen, M. Lazzeri, and F. Mauri, "Hidden polymorphs drive vitrification in B₂O₃," *Nat. Mater.* **11**(11), 925–929 (2012).
 14. W. Vogel, *Glass Chemistry* (Springer-Verlag, 1994).
 15. J. Cao, B. Pommellec, F. Brisset, A. L. Helbert, and M. Lancry, "Angular dependence of the second harmonic generation induced by femtosecond laser irradiation in silica-based glasses: variation with writing speed and pulse energy," *World J. Nano Sci. Eng.* **05**(03), 96–106 (2015).
 16. B. Pommellec, M. Lancry, C. Fan, A. Erraji-Chahid, and P. Kazansky, "Asymmetric orientational femtosecond laser writing detected in several properties in various glasses," *Advances in Optical Materials*, OSA Technical Digest (CD) (Optical Society of America, 2011), paper AIFB2.
 17. K. Veenhuizen, D. N. Sean McAnany, B. Aitken, V. Dierolf, and H. Jain, "Fabrication of graded index single crystal in glass," *Sci. Rep.* **7**(1), 44327 (2017).
 18. J. Cao, B. Pommellec, F. Brisset, A.-L. Helbert, and M. Lancry, "Tunable angular-dependent second-harmonic generation in glass by controlling femtosecond laser polarization," *J. Opt. Soc. Am. B* **33**(4), 741–747 (2016).